Thermal Cycling of Thermoelectric Generators: The Effect of Heating Rate

R. Merienne, J. Lynn, E. McSweeney, S. M. O'Shaughnessy[1]

Department of Mechanical & Manufacturing Engineering, Parsons Building, Trinity College Dublin, Ireland.
[1]Email: oshaugse@tcd.ie
[1]Tel: +353 1 896 1778

Abstract

Thermoelectric generators, or TEGs, are solid state devices which can convert heat directly into electricity according to the Seebeck effect. When thermoelectric generators are subjected to thermal cycling they can undergo severe performance degradation. In this study, an experimental rig is constructed which is capable of thermally cycling the heat delivered to commercially available thermoelectric generators. An experimental investigation is undertaken to elucidate the effects of the cycling and heating rate on the power generation performance of the generators over time. Three generator modules of the same specifications were subjected to different heating rates. The figure of merit, the electrical power output, the effective Seebeck coefficient and the internal resistance of the generators are measured to assess the evolution of the modules' performance over 600 heating and cooling cycles. It is determined that all thermoelectric generators display power generation performance reductions, and that faster thermal cycling rates lead to both faster performance degradation and an overall greater performance drop. It is observed that the reduction of the figure of merit and power generation performance is primarily due to the increase of the internal resistance of the thermoelectric generators.

Keywords

Thermoelectric generator; electricity generation; thermal cycling; life cycle analysis; variable heating rate; thermal stress;

1. Introduction

Thermoelectric generators (TEGs) are solid state semi-conductor devices which convert heat directly into electricity via the Seebeck effect. Despite their low efficiency of <7%, the absence of moving parts has been said to make TEGs reliable power generators when operated under stable thermo-mechanical conditions [1]. TEGs are widely employed in a variety and growing number of applications, including but not limited to space exploration [2], automotive heat recovery applications [3], remote power applications [4], domestic power generation [5, 6] and industrial waste heat recovery [7, 8]. However, when operated in an environment that undergoes thermal cycling, the power generating performance of TEGs can be adversely affected. The purpose of this study is to investigate how the thermal cycling rate affects the electricity generating performance and internal properties of commercially available TEG modules.

Published literature on this topic appears to be limited. More recent TEG thermal cycling studies have focused on thin film generators (e.g. Mirhosseini et al. [9]) rather than more standard TEGs, but comparisons between the two types are not valid because of the significant difference in size, construction, and materials used. Experimental investigations of standard TEGs typically involve a sample placed between a heat source and sink with the cold side of the TEG maintained at a constant temperature and the hot side temperature cycled, such as the study by Chen and Lee [10]. Hori et al. [11] assessed the influence of thermal cycling on the performance of bismuth telluride (Bi_2Te_3) TEGs. Three modules were investigated, each consisting of thermoelectric elements with a different cross-sectional area. In their thermal cycling regime, the cold side temperature of the TEGs

was maintained at 30°C whereas the hot side temperature was varied between 30°C and 180°C. The duration of the heating and cooling periods was not indicated however.

It was found that the performance of each TEG was adversely affected by the thermal cycling and the generated power was observed to decrease with an increasing number of cycles. Moreover, the number of cycles before a sudden drop in performance, called 'breakdown', was dependent on the cross-sectional area of the thermoelectric elements in the TEGs, with larger area elements having a superior lifespan.

Gao et al. [12] used nanostructured interfaces located directly on the thermoelectric materials in TEGs in an attempt to reduce the severe thermomechanical stresses due to the significant mismatch of the thermal expansion coefficient at the interface. The effect of 100 thermal cycles was studied with the temperature in the tests varying between 30°C and 200°C with a cycle time of approximately 6 minutes. The results on the effect of thermal cycling on TEG performance were inconclusive, with the authors stating that the difference in the module's thermal resistance after 100 cycles was within the error range and concluding that further studies were needed to confirm the effects of thermal cycling.

Hatzikraniotis et al. [13] studied the effect of thermal cycling on a 25 mm x 25 mm Bi_2Te_3 TEG consisting of 31 thermoelements. A cycle consisted of a ~6-minute-long heating stage, a ~5-minute period of constant operation and a ~20-minute-long cooling stage. The TEG was subjected to 6000 cycles with a hot side temperature varying between 30°C and 200°C and a

cold side temperature maintained constant at 24°C. The power generated by the TEG was measured during each cycle and during the constant operation phase an external resistive load was connected. Excluding a power drop in the first 50 cycles which the authors attributed to a deterioration of the thermal grease used, the total power drop after 6000 cycles was approximately 14%. Furthermore, the dimensionless figure of merit was found to decrease from ZT=0.74 to ZT=0.63, the Seebeck coefficient decreased by 3.8% and the internal resistance of the module increased by 16.1%. SEM Scanning electron microscope imaging of the module pre and post thermal cycling showed the development of micro-cracks in the TEG layers.

Barako et al. [14, 15] applied a square wave voltage to the TEG to heat one side while the other was maintained at 23°C by a heat sink. The temperature of the hot side of the TEG could be varied between -20°C and 146°C. According to the authors, this cycling configuration is representative of the thermomechanical stresses in TEGs whether they are in power generation or cooling mode. The authors observed a decrease of the resulting hot side temperature range from (+146°C; -20°C) to (+40°C; +20°C) at 45000 cycles, proof of the TEG module failure. Similarly, the figure of merit was observed to decrease over the cycle and a large increase in the internal resistance was observed which was attributed to the formation of micro-cracks at the TEG leg/solder interface.

Park et al. [16] used two TEG modules thermally in series as the hot source for their TEG thermal cycling rig. A third TEG module (i.e. the module under test) was subjected to hot side temperature cycling between 30°C and 160°C every 3 minutes, with the cold side temperature held constant at 20°C by a cooled copper heat sink. To evaluate the performance of the module under test, the authors measured the dimensionless figure of merit every 1000 cycles. After 6000 cycles it was observed that the figure of merit decreased by 8% and the internal resistance increased by 2%. Moreover an 11% drop in the power generated was observed.

In their TEG thermal cycling study, Tatarinov et al. [17] constructed a measurement setup with a vacuum chamber to exclude convective losses. Optical and infrared measurements of the TEG were performed during testing. During the thermal cycling test, the cold side temperature was constant at 30°C and the hot side was periodically varying between 50°C and 250°C with a cycle duration of approximately 11 minutes. After 340 cycles, the power output was observed to decrease by 11% while the total system energy conversion efficiency remained constant. The authors concluded that the degradation of the TEG was mostly due to the degradation of the thermal contact.

Unlike many of the studies mentioned above, the experimental rigs constructed by de Cerqueira Veras et al. [18] and Tenorio et al. [19] can vary the temperature on both sides of the TEG, which, according to the authors, enables the evaluation of TEGs under more realistic operational conditions. The test platform consists of a TEG positioned between two other thermoelectric modules acting as heater and cooler periodically. Positive or negative temperature gradients could be applied across the module; one side of the test TEG becoming alternatively the hot side and then the cold side. During the thermal cycling test, the temperatures of each side of the TEG were alternatively set to 20°C and 40°C. The duration of each cycle was approximately 15 minutes. ZT was determined to have decreased by 7.14% after just 100 cycles. Similar results were observed in a later study by Tenorio et al. [20] after 127 cycles.

A study by Ding et al. [21] appears to be only one to investigate the effect of different cycling operating conditions on TEGs. In the study, the authors observed the evolution of the power generation performance and the open circuit voltage in response to two different cycling conditions. The heating and cooling times were equal to 15 minutes in both configurations, but the heating power was varied between tests at 80 W and 160 W respectively, which dictated the maximum hot side temperature reached. After 500 cycles for both conditions, the authors observed that at 80 W the performance of the TEG remained constant. However, after 300 cycles at 160 W abnormal fluctuations in the open circuit voltage were detected, which, according to the authors, were not caused by instrument error but possibly by weakening of the solder connections within the module. The authors stated that thermal cycling with hot side temperatures near 150°C adversely affects the TEG performance and can lead to TEG malfunction.

Recently, Patel et al. [22] performed a long-term study of the effects of power-cycling on multiple samples of a Peltier module with 127 thermoelements. After 168 days of operation consisting of duty cycles of 45 minute ON periods and 5 minute OFF periods, the general trends displayed a small increase in module electrical resistance and a corresponding small decrease in the figure of merit. It should be noted that the maximum average temperature of the samples was limited to less than 45 °C during the study, which may explain the longevity.

The limited published studies on the effects of thermal cycling on TEGs suggest that further research is required to elucidate TEG performance effects, in particular to quantify power output degradation and how this may be linked to the operating conditions. It appears that no previous studies have investigated the effect of the heating rate whilst operating between consistent hot and cold side temperatures for multiple samples of the same generator. In this study three samples of the same TEG model number are subjected to different heating profiles whilst operating between the hot side temperature limits of 50°C and 165°C. The samples, named henceforth as TEG A, TEG B and TEG C, were subjected to 600 thermal cycles and performance characterisation tests at specified intervals. The results of this study are of interest to engineers, researchers, physicists and designers of thermal systems or

applications that incorporate thermoelectric modules operating under transient thermal conditions, such as automobile and fuel cell waste heat recovery, solar thermoelectric generation, refrigeration, flow and heat flux sensors, and industrial cogeneration.

2. Thermoelectric theory & modelling

The Seebeck effect is described by Rowe [23]. Initially the conductors have a uniform distribution of charge carriers, however when subjected to a temperature gradient, the free carriers at the hot end tend to diffuse to the cold end, because their kinetic energy is higher. The accumulation of charge results in a back electromotive force. If the temperature gradient across the junctions is maintained, the open-circuit voltage V_{OC} is generated when no current flows:

$$V_{OC} = \alpha \Delta T_{TEG} = \alpha (T_H - T_C) \qquad (1)$$

In Equation 1, T_H and T_C are the temperature of the hot and cold junctions respectively. The Seebeck coefficient α is equal to the difference of the Seebeck coefficient of the two semiconductor materials. The thermoelements within the TEG are connected electrically in series and thermally in parallel as shown in Figure 1, and the shunts are made of a good electrical conductor, usually copper. The thermoelements are placed between two ceramic plates which have a low electrical conductivity and relatively high thermal conductivity.
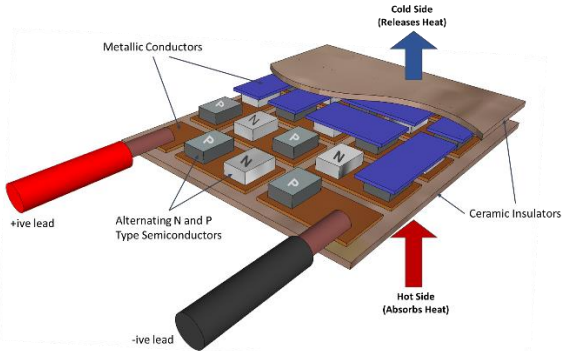

Figure 1: Thermoelectric generator

The operation of a thermoelectric generator requires both a heat source and sink to maintain a driving temperature difference between the faces of the TEG. The heat source maintains the temperature at the 'hot' face of TEG module while the heat sink absorbs the heat from the TEG maintaining the 'cold' face temperature. The ability of a thermoelectric material to efficiently produce electricity depends on its internal properties. The materials need to be a good electrical conductor to avoid electron scattering, must have a low thermal conductivity to decrease thermal losses from the junctions and the Seebeck coefficient must be as high as possible to have a significant V_{OC} [24]. The performance of a thermoelectric material can be determined by the value of its figure of merit, Z:

$$Z = \frac{\alpha^2 \sigma}{\lambda} \qquad (2)$$

In Equation 2, σ and λ represent the electrical and thermal conductivity of the material respectively. The figure of merit is often expressed in the dimensionless form ZT, where T represents the average temperature of the module. The materials with the best figure of merit are heavily doped semiconductors which can be both p- and n-type doped, so the same material can be used on both sides of the junctions [24]. Bismuth telluride generators have the best figure of merit ($\approx 3.4 \times 10^{-3}\ K^{-1}$) but are limited to low operating temperatures, typically $< 250°C$.

Using a one-dimensional model of a single thermoelement of density, ρ, length L and cross-sectional area A, the internal electrical resistance, R, and the thermal conductance, K, are defined by Equations 3 and 4 respectively.

$$R = \frac{2\rho L}{A} \qquad (3)$$

$$K = \frac{2\lambda A}{L} \qquad (4)$$

The model is based on the equations describing the Seebeck, Fourier and Joule effects. Using the standard model proposed by Hodes [25], the rate of heat absorbed, Q_H, and heat rejected, Q_C, can be expressed as follows:

$$Q_H = K(T_H - T_C) + (\alpha_p - \alpha_n)IT_H - \frac{RI^2}{2} \qquad (5)$$

$$Q_C = K(T_H - T_C) + (\alpha_p - \alpha_n)IT_C + \frac{RI^2}{2} \qquad (6)$$

Here I is the current through the thermoelement, and α_p and α_n are the Seebeck coefficient of the p- and n-type doped semiconductor materials respectively. The electrical power generated by the thermoelement is:

$$W = V \times I = Q_H - Q_C \qquad (7)$$

Or, equivalently:

$$W = I(\alpha_p - \alpha_n)(T_H - T_C) - RI^2 \qquad (8)$$

Dividing by the current and combining the individual Seebeck coefficients into one parameter $\alpha = \alpha_p - \alpha_n$ gives:

$$V = \alpha(T_H - T_C) - RI \qquad (9)$$

Equation 9 gives the relationship between the voltage and the current at a set temperature difference. When the thermoelement is connected to an external load, the TEG power is equal to the electrical power in the external load, $I^2 R_L$, and from Equation 8, the current is:

$$I = \frac{\alpha(T_H - T_C)}{R + R_L} \qquad (10)$$

The combination of Equations 9 and 10 gives the power as a function of the temperature difference, internal resistance and load resistance. From Equation 11 it can be seen that the maximum generated power is obtained when the external load matches the internal resistance of the module, i.e. when $R_L = R$. Equation 12 shows that in order to obtain the greatest power possible, the thermoelements within the TEG should be as short as possible with the largest cross-sectional area possible.

$$W = (\alpha \Delta T)^2 \frac{R_L}{(R + R_L)^2} \qquad (11)$$

$$W_{MAX} = \frac{(\alpha \Delta T)^2}{4R} = \frac{A(\alpha \Delta T)^2}{8\rho L} \qquad (12)$$

2.1 Failure mechanisms

TEGs have low heat-to-power conversion efficiencies so the temperature difference across the modules must be significant to produce significant electrical power. This aspect, coupled with the requirement for short thermoelements, means that many TEGs used for power generation experience large thermal gradients. Additionally, there are mismatches of the thermal expansion coefficients of the materials within the TEG, the consequence of which is the formation of high thermomechanical stresses inside the module. Moreover, during thermal cycling the fluctuation in the temperature gradient induces additional thermal stresses that can create micro-cracks at the interface where the materials meet and, in the pellet, [14]. Under thermal cycling, the electrical resistance of the TEG increases, resulting in a decrease of the figure of merit and the power output. The thermal resistance is also increasing because of the formation of micro-cracks at the interface. The consequence is that the effective temperature difference across the semiconductor material decreases and therefore the power output decreases [26].

The geometry of the semiconductor pellets certainly plays a role in the rate of performance degradation, but the lack of consistency in the test parameters and associated results in the literature makes it difficult to draw any meaningful conclusion. Heating and cooling rates, cycle temperature limits, TEG size, number of pellets per TEG, no. of cycles completed, and no. of samples tested vary from study to study. For example, in ref. [11], experiments using 47.5 mm x 47.5 mm TEGs with 49 thermoelements showed that TEGs with larger area pellets display a slower rate of degradation. In ref. [13] 6000 cycles were completed with a 25mm x 25mm TEG containing 31 thermoelements, resulting in a ZT reduction of ~15%. Whereas, in ref. [20], a 40 mm x 40 mm TEG containing 127 thermoelements (similar to the current study), displayed a 7% reduction in ZT value after just 127 cycles.

Cracks can form within pellets in a direction parallel or perpendicular to the interfaces. Moreover, some defects such as voids and cracks can be present pre-cycling as a consequence of the manufacturing processes. Considering these factors, it is expected that significant variation of performance in response to thermal cycling would be obtained when testing similar modules from different manufacturers.

2.2 The Effective Seebeck Coefficient model

Zorbas et al. [27] and Hsu et al. [28] used a method to determine the internal properties of a TEG under real test conditions by considering thermal contact effects between the material interfaces and the actual properties of the materials in the TEG. Using this method, the open circuit voltage V_{OC} can be obtained from the y-intercept of a plot of the TEG voltage versus current. The negative of the slope of the line is equal to the internal resistance of the module. Figure 2 shows such an example for TEG A before thermal cycling commenced. In this case V_{OC} = 5.68 V and R = 1.88 Ω. The effective Seebeck coefficient α_{eff} is then calculated using Equation 13.
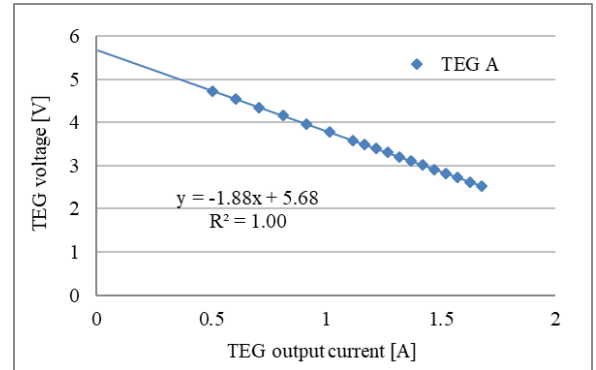

Figure 2: Pre-cycling characterisation test performed on TEG A, showing the extrapolated open circuit voltage and internal resistance values.

$$\alpha_{eff} = \frac{V_{OC}}{T_H - T_C} \qquad (13)$$

2.3 TEG module selection

The chosen TEG is the TG-127-200-24 supplied by Thermalforce. The specifications for the TEG are given in Table 1. The thermoelements of this TEG are made from Bi_2Te_3 which has a maximum Seebeck co-efficient at approximately 50 °C. If the TEG is maintained below its maximum operating temperature, a larger temperature difference will of course produce greater power. However, as the average temperature of the TEG increases, the potential to produce power will also decrease. Thus, for the same temperature difference, maintaining the TEG at a lower average temperature will generate more power [29].

Table 1: Supplier's TEG specifications at $T_H = 150°C$ and $T_C = 30°C$, excl. thermal contact resistances [30]

Type	Bi_2Te_3
Max. hot side temperature	200°C
Dimensions	40mm x 40mm
Number of thermoelements	127
Open circuit voltage	6.692 V
Internal resistance	1~1.5Ω
Matched load output voltage	3.146 V
Matched load output current	2.061 A
Matched load output power	6.485 W
Heat flow hot side	159.5 W
Heat flow cold side	153.9 W

3. Experimental setup

A photograph of the exposed experimental rig is provided in Figure 3. Some pieces of insulation have been removed for visual access. As in the majority of TEG thermal cycling studies, the experimental rig consists of a TEG module sandwiched between aluminium heating and cooling blocks. The rig is designed to accommodate TEGs with cross-sectional areas from 20mm x 20mm up to 56mm x 56mm. Calibrated type-K 1.5 mm diameter stainless steel sheathed grounded thermocouples are placed in both blocks at a distance of 1.5 mm from the aluminium-TEG interfaces to enable the approximate TEG face temperatures to be measured. The true temperature difference across the thermoelements of the TEG will be smaller than that measured by the thermocouples. The rig is enclosed by 25mm thick Duratec 750 calcium silicate insulation which has low thermal and electrical conductivity and can withstand large applied pressure.

Clamping pressure is an important parameter that affects TEG performance [31]. In this study a clamping system consisting of four M6, 150 mm long bolts and hexagonal nuts is used. The clamping pressure of 1 MPa is set by applying the same torque of 0.5 Nm on each nut using a calibrated narrow range torque screwdriver. This torque setting is checked periodically throughout testing. The rig has been designed to eliminate any direct thermal pathways through the bolts, yet the clamping pressure may be slightly affected by the expansion of the bolt and heating block during thermal cycling. Some loosening could be expected over time. To protect against this, series pairs of Belleville washers are used in accordance with TEG manufacturers' guidelines. Not shown in Figure 3 are the top and bottom aluminium plates against which the clamping force is applied.
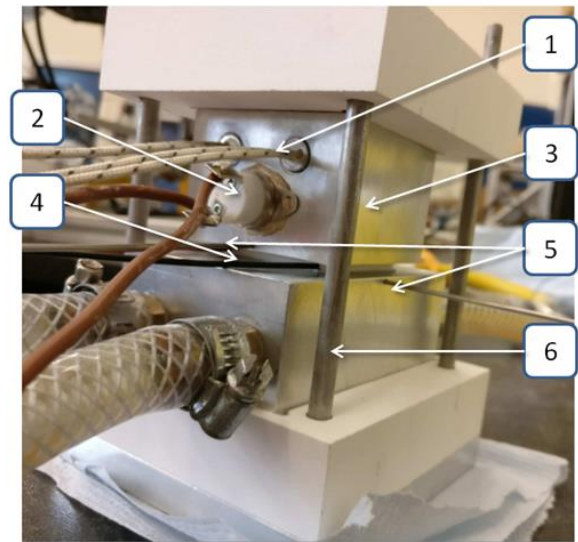

Figure 3: TEG cycling experimental rig showing (1) Cartridge heater, (2) Thermostat, (3) Heating block, (4) TEG, (5) Thermocouples, (6) Cooling block.

Heat is supplied to the heating block by two 2" long x 3/8" outer diameter 200 W cartridge heaters, powered by an Elektro-Automatic PS8360-10T power supply which is controlled by USB connection to a PC running the software LabVIEW. A thermostat placed on the heating block provides a physical safety mechanism that disconnects the cartridge heaters when the heater block temperature reaches 200°C.

Ming [32] showed that uneven temperature distributions on the hot TEG face can lead to large increases in the thermal stresses induced. Therefore, to determine the required thickness of the heating block, ANSYS steady state and transient simulations are carried out to check the ability of the block to generate an even temperature on the hot face of the TEG. A further design consideration is that the thickness of the heating block should be reduced as much as possible to limit the thermal inertia so that fast heating times may be achieved. The computational mesh and sample thermal profile are shown in Figure 4. In the simulations a fixed temperature of 30°C is applied to the upper surface (i.e. the cold face) of the TEG. To simulate the ceramic insulation, a convection heat transfer coefficient of 2 W/m²K is applied to the sides and the bottom of the heating block. The cartridge heaters are replicated by a 37 kW/m² heat flux boundary condition corresponding to 120 W of heat input. Thermal contact resistances are neglected. The material properties used for the TEG are provided by the manufacturer. With a heating block thickness of 40 mm, a uniform temperature distribution on the heating block face in contact with the TEG is attained, as seen in Figure 4.
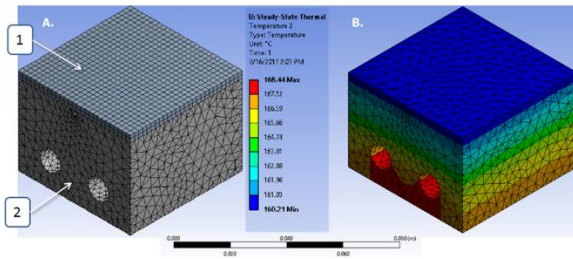
Figure 4: ANSYS simulation to determine the TEG cold side temperature profile (1) and the optimum heating block thickness (2), showing (A) the computational mesh, and (B) thermal profile using a block thickness of 40 mm.

The cooling block temperature is maintained at a user selected setpoint using a simple design. Water is supplied by a Fisher Scientific Isotemp recirculating chiller and flows through two channels in the cooling block before returning to the chiller reservoir. The chiller setpoint is also controlled by LabVIEW for convenience.

3.1 Data acquisition & measurement

The thermocouple measurements are recorded using a National Instruments (NI) 9211 data acquisition module (DAQ). These temperature readings are also used as inputs to a LabVIEW virtual instrument (VI) which controls the thermal cycling routine. The TEG voltage is recorded by a NI-DAQ 9215. The TEG current is not directly measured; rather it is calculated from the measurement of the voltage drop across a 0.04 Ω sense resistor. This method has been used extensively in previous studies by the authors, for example in ref. [33]. The voltage drop across the sense resistor is small (100 mV max.), such that a 24-bit NI-9219 DAQ can be used because of its better resolution in the range ± 125 mV. All DAQ modules are connected to LabVIEW via an NI-cDAQ 9174 chassis.

A BK precision 8540 variable electronic load is used to consume the power generated by the TEGs under test. This device can operate in various modes: CC (constant current), CV (constant voltage) and CR (constant resistance). Only the CC (constant current) mode is used in this study as the constant resistance mode was found to be unstable at low resistances (<0.5Ω), and because the internal resistance of the TEGs was expected to increase with thermal cycling. Unfortunately, this device cannot be controlled by PC, which limits the complete automation of the experiment.

3.2 Experiment control

A bespoke LabVIEW VI controls the heater power and the chiller setpoint temperature using PID methods, effectively enabling control of the temperature of the blocks on both sides of the TEG and therefore the heating and cooling times. The VI is based on a state machine architecture as shown in Figure 5, and can maintain heating times and hot side temperatures with excellent consistency during the thermal cycling. The VI can also maintain a steady temperature difference throughout the characterisation testing. The VI contains some safety features which prevent the hot and cold side temperatures from exceeding predetermined limits. The VI records the TEG hot and cold side thermocouple temperatures, the TEG voltage and current, the external load voltage and current and the heating and cooling time for each cycle.
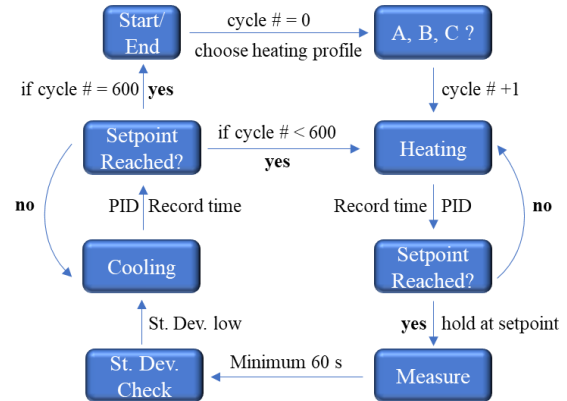

Figure 5: State machine flow diagram

3.3 Experimental procedure

Three TG-127-200-24 TEGs, identified as TEG A, TEG B and TEG C, are subjected to thermal cycling regimes with three different heating times; all other test parameters are unchanged. Each TEG is subjected to 600 cycles, where one cycle consists of a predetermined heating and cooling period. Three different tests, described below, are performed on each TEG to assess their performance.

3.3.1 Thermal cycling test

The hot side temperature cycles between 50 °C and 165°C. These temperatures are chosen to maintain the TEG below the maximum operating temperature of 200°C and to have a reasonable cooling time. Once the TEG hot side temperature reaches the setpoint of 165°C, the TEG temperature difference is maintained for a minimum of 60 seconds to account for any fluctuations due to the Peltier, Joule and Thomson effects. During this phase, 100 samples of each measured parameter are recorded into a data array. The VI initiates the cooling phase only when the standard deviation of the hot side temperature is ≤0.1°C, its mean equal to 165 ± 0.2°C and if the measurement time has reached 60 seconds. In practice, during this phase the measurement time is always equal to 60 seconds. The cooling settings remain constant for all thermal cycling tests. The chiller is set to maintain the water circulating in the cold block at 20°C. The cooling time is approximately constant for each TEG at 9 minutes.

The power produced by the TEG is consumed by an electronic load set to constant current mode at 1.4 Amps during all stages of the cycle. In practice, as the TEG temperature difference increases/decreases during a thermal cycle, the TEG voltage (and therefore the voltage across the terminals of the electronic load) also increases/decreases. The approximate TEG temperature

difference, the TEG voltage and current are measured during this test as are the external load parameters.

During the PID tuning phase, three repeatable heating times were decided upon and the relevant parameters are shown in Table 2. The LabVIEW VI performs 50 cycles after which the experiment cools to ambient temperature before user intervention is required to perform the characterisation test described in the next section. Figure 6 shows the three different thermal cycling profiles for TEGs A, B and C. Each cycle displays a slight overshoot of the setpoint temperature of < 2°C before the measurement phase at constant temperature begins.

Table 2: Power control settings for each TEG during thermal cycling

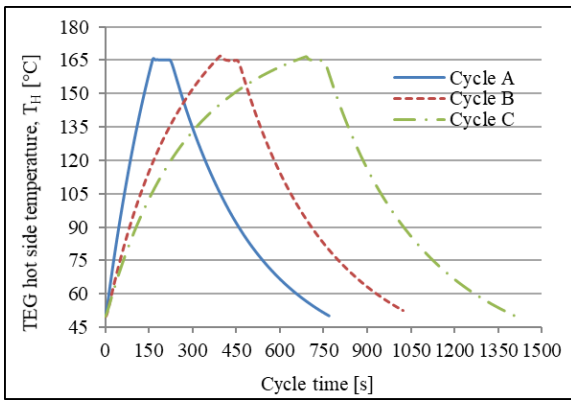| TEG	Heating time [s]	Cooling time [s]	Heater power [W]	Cycle duration [s]
A	160	540	390	760
B	390	540	238.5	990
C	720	540	198	1320

Figure 6: Thermal cycling profiles for the 3 TEGs

For the heating cycle, a constant heating power is applied until the calibrated hot side thermocouple reading equals the set point temperature minus an adjustment temperature. Only at this point is PID control used to reach and maintain the setpoint temperature. This method was chosen because preliminary testing showed that PID control is more effective when activated when the temperature is close to or higher than the set point temperature. The PID parameters were determined using the Ziegler–Nichols tuning method for fast performance [34]. To determine the constant heating powers, adjustment temperatures and PID values, a tuning phase with an uncycled TEG was performed. The uncycled TEG was the same model as the TEGs used in the study. The PID settings for controller gain, K_u, proportional gain, K_p, integral time t_i, and derivative time, t_d, are provided in Table 3 along with the associated adjustment temperatures. For reference, the heating time for TEG B is similar to the one used by Hatzikraniotis et al. [13] while that for TEG C more closely resembles the real-world conditions mentioned in Deasy et al. [35].

Table 3: PID settings and adjustment temperature values for each thermal cycling profile

TEG	K_U [-]	K_P [-]	t_I [s]	t_D [s]	Adjustment temp. [°C]
A	160	96	14.1	3.5	+1.5
B	160	96	14.1	3.5	-1.5
C	160	96	14.1	3.5	-1.5

3.3.2 TEG characterisation test

The purpose of the TEG characterisation test is to measure the internal properties of the TEG and it is performed for each TEG before thermal cycling begins and after every 50 cycles. During the test, the TEG is maintained under a constant temperature difference while the current drawn by the electronic load is increased from 0 A (open circuit condition) to 1.65A in steps of 0.05A or 0.1 A. The variation of current drawn from the TEG induces a slight variation of the cold side temperature of ±2°C. To maintain a constant ΔT_{TEG}, the hot side temperature is set at $T_C + 130$°C. In practice, the hot side temperature varies between 161°C and 163 °C. The maximum power point is obtained when the load resistance matches the internal resistance of the TEG. Figure 7 plots the power versus resistance curves for each of the TEGs prior to thermal cycling, and Table 4 displays the relevant results of the pre-cycling characterisation tests. The data shows that prior to thermal cycling, TEGs A and B perform very similarly. TEG C displays similar trends but produces less power in accordance with its lower Seebeck coefficient. The difference in performance was not attributed to variations in clamping pressure as this was checked at several stages during the test. The data shows that the same, new TEG model can have varying performance.
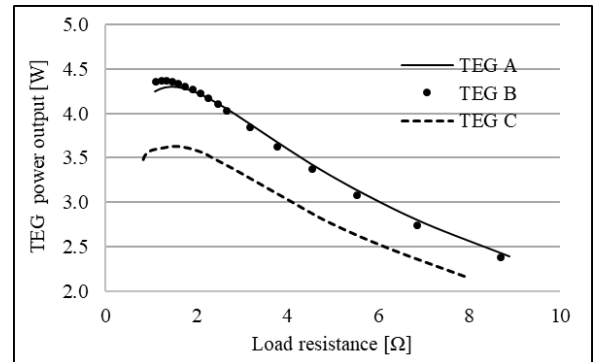

Figure 7: Pre-cycling TEG power vs load resistance, showing the maximum power point at apparent TEG temperatures of $T_H \approx 161$°C and $T_C \approx 30$°C.

Table 4: Pre-cycling TEG characterisation test results

TEG	V_{OC} [V]	$\alpha_{eff, average}$ [V/K]	R [Ω]	W_{MAX} [W]
A	5.68	0.0437	1.88	4.29
B	5.62	0.0432	1.81	4.36
C	5.26	0.0405	1.91	3.66

3.3.3 Figure of merit test

The Harman method is a simple method used to determine the figure of merit at room temperature [36]. A small DC current is applied to a TEG, creating a small temperature difference due to the Peltier effect and a small voltage across the terminals. The generated voltage has both an electrical component, V_{Joule}, due to the current circulating through the internal resistance of the module and another, $V_{Seebeck}$, due to the temperature difference induced by the Peltier effect [20]. This method is derived from an analysis of a single thermoelectric pellet. For brevity, the dimensionless figure of merit is given by Equation 14.

$$ZT = \frac{V_{Seebeck}}{V_{Joule}} \qquad (14)$$

To perform the Harman method, the TEG is connected to a DC power supply and to an external load used in constant current mode to maintain a constant current of 10 mA in the circuit. When the system reaches a steady state, which is determined by analysis of the stability of the TEG voltage generated, the power supply is turned off and the voltage is observed to decrease until the TEG reaches a thermal equilibrium. V_{Joule} is determined from the difference between the steady state voltage and the residual Seebeck voltage and the dimensionless figure of merit is calculated using Equation 14. Figure 8 shows an example of Harman method testing performed for TEG A in this study.
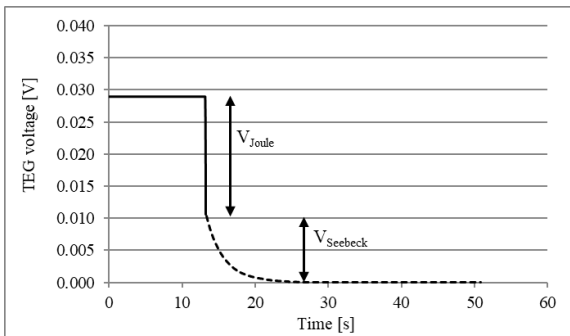
Figure 8: Sample Harman method testing for TEG A

The Harman method described can only be performed when the TEG is removed from the experimental rig, limiting its use to pre and post-cycling. This test is repeated a minimum of ten times for each TEG and those results are averaged to ensure a more representative ZT.

3.4 Uncertainty analysis

To ensure precision in the measurement data, standard deviation criteria are applied to thermocouple and voltage measurements before the VI enables subsequent measurement phases. Additionally, a measurement uncertainty and propagation analysis were conducted on all reported variables and the associated maximum uncertainties are reported results are in Table 5.

Table 5: Maximum uncertainty for reported variables

Description	Max. uncertainty
TEG voltage	± 3 mV
TEG current	± 24 mA
TEG power	± 66 mW
TEG electrical resistance	± 82 mΩ
TEG temperature diff.	± 0.4 °C
Eff. Seebeck coefficient	± 157 µV/K
Figure of Merit	± 0.152

4 Results and discussion

4.1 Thermal cycling test results

Figure 9 plots the evolution of the measured TEG power at a current draw of 1.4 A from the electronic load. The data is recorded at the end of the measurement period between the heating and cooling phases of each cycle. Clearly, for all TEGs the power produced at 1.4 A decreases with an increasing number of cycles. The power generated by TEG A is observed to decrease almost linearly, whereas the power generated by TEG B and C decreases more gradually. These results show that at a constant current demand of 1.4 A from the electronic load, all TEGs undergo performance degradation under thermal cycling which is in accordance with the literature. However, the TEGs appear to be affected differently by the thermal cycling. To compare the effect of the different cycling regimes, the power generated by each TEG is normalised relative to the power that each TEG produced during the measurement phase of cycle 1. The results are shown in Figure 10.
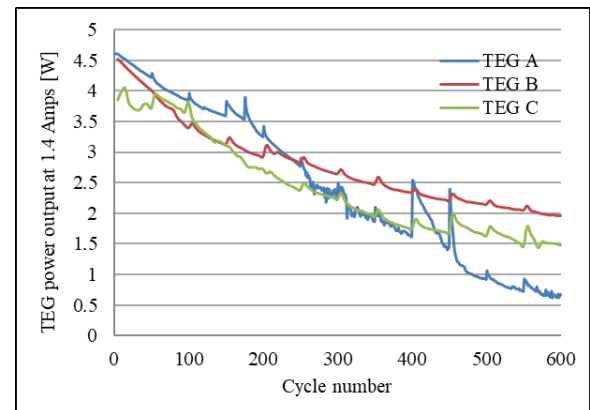
Figure 9: Power produced by the three TEGs during the measurement period of every thermal cycle at a constant current setting of 1.4 A
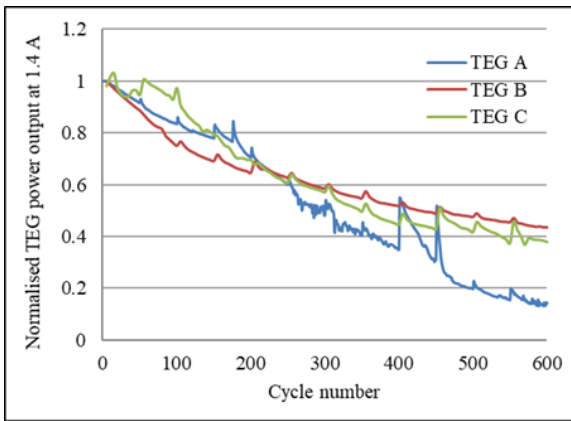
Figure 10: Normalised power produced by the three TEGs during the measurement period of every thermal cycle at a constant current setting of 1.4 A

Employing a constant current mode induces an increasing mismatch between a TEG's internal resistance and the resistance of the external load, which is reflected in Figure 9 and Figure 10. Indeed, the external load resistance decreases over the cycling tests because the TEG power decreases, whereas the internal resistance of the TEG changes during each cycle and should display an overall increase according to the literature. For this reason, the maximum power point is also measured during the characterisations tests after every 50 cycles, the results of which are displayed in Section 4.2.1.

4.1.1 The recovery effect
As detailed in Section 3.3.1, 50 thermal cycles take place before user intervention is required to perform the characterisation test. When thermal cycling resumes, there appears to be a recovery effect in terms of the power produced by the TEG. This is evidenced by the frequent spikes in power every 50 cycles in Figure 9 and Figure 10. This phenomenon happened every time the TEG was not subjected to a thermal gradient for a relatively long period of time, for example, when the 50th cycle finished during the night. No references to this phenomenon were found in the literature. It is believed that this phenomenon may be due to two different causes. Firstly, as mentioned in the literature review, during thermal cycling micro-cracks are forming between the TEG elements and the solder legs due to the mismatches of the thermal expansion coefficient. During the idle period of the rig there is no thermal gradient, and the contact between the TEG elements and the solder could be reformed to some degree. Another possible cause for this behaviour is the clamping system. During the heating portion of the first cycle following each characterisation test, i.e. cycles 1, 51, 101 etc., the heating block expands whereas the clamping bolts are still cold owing to the insulating plates. However, after several thermal cycles the temperature of the clamping bolts increases by a small amount which may lead to a slight loosening of the bolts, reducing the total clamping pressure and therefore reducing power output. The clamping bolts were checked periodically using the calibrated torque screwdriver with a resolution of 0.05

Nm, however it must be noted that the manufacturer's stated accuracy of this device is approximately ±6%. The cause for this recovery effect is therefore not yet fully understood and requires further investigation. Nevertheless, some clear trends can be observed from the data.

4.1.2 Heating time analysis
The heating (and cooling) times were recorded for each cycle. A significant change in the heating time would reflect a similarly significant change in the thermal resistance of the system, particularly of the TEG. The normalised heating times over the 600 cycles are shown in Figure 11. For image clarity, every 5th data point is shown. The heating time for each cycle was normalised compared to the average heating time. The data is refined by removing the heating time of the first cycle following a characterisation test, since in some cases the experiment must heat up initially from ambient temperature to 165°C instead of heating up from 50°C to 165°C for the following cycles. The trends indicate that the heating time very slightly decreases with increasing number of cycles. This is in agreement with results found by Tachibana et al. [26] who showed an increase in the thermal resistance of the thermoelectric generator due to thermal cycling, which leads to a reduction of the heat transfer through the TEG and thus shorter heating times.
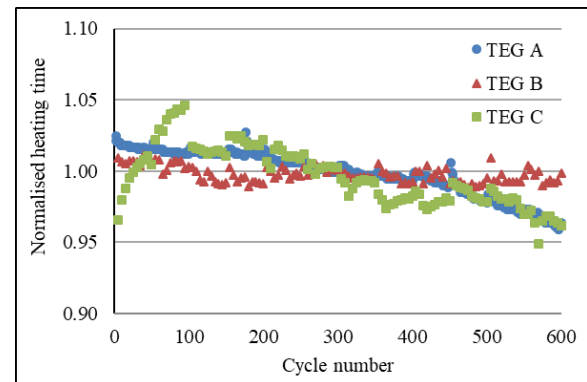

Figure 11: Normalised heating time evolution for each cycling regime

4.2 TEG characterisation test results
This section describes the results obtained from TEG measurements taken at the beginning and every 50 cycles until the end of the thermal cycling periods.

4.2.1 Maximum power output
Figure 12 plots the normalised power production versus cycle number. The maximum power produced by each TEG is normalised relative to the maximum power produced during the pre-cycling characterisation tests (cf. Table 4). It is evident from these curves that the maximum power generated by each TEG decreases with an increasing number of thermal cycles. In accordance with the thermal cycling tests, the trends are different for each TEG. The TEG undergoing the fastest cycling, TEG A, exhibits a linear decrease in the normalised maximum power output, while TEGs B and C exhibit

more complex polynomial trends. The figures consolidate the hypothesis that thermal cycling adversely affects the power generation performance of the TEG and that faster thermal cycling results in greater performance reduction. The total maximum power drop is approximately 61% for TEG A, 36% for TEG B and 29 % for TEG C. Interestingly, despite TEG A showing the greatest overall drop in maximum power output, during the first 100 cycles TEG B displays the largest power degradation. Contrastingly, TEG C shows almost no change in the first 100 cycles.
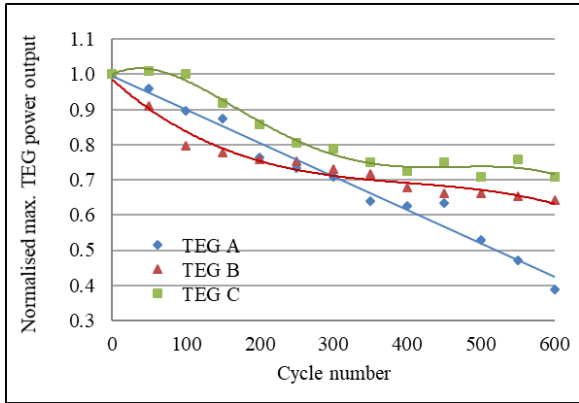

Figure 12: Evolution of the normalised maximum power for each TEG over 600 thermal cycles

4.2.2 Internal resistance, R

Figure 13 plots the normalised internal resistance at $T_H \approx 161°C$ and $T_C = 30°C$ for each TEG. As before, the data is normalised relative to the internal resistance values displayed in Table 4. It is evident that the internal resistance of all TEGs increases with an increasing number of cycles, as expected. For TEG A, the final internal resistance is more than doubled compared to its pre-cycling value while the final internal resistance for TEGs B and C are close to 1.7 times their respective initial values.
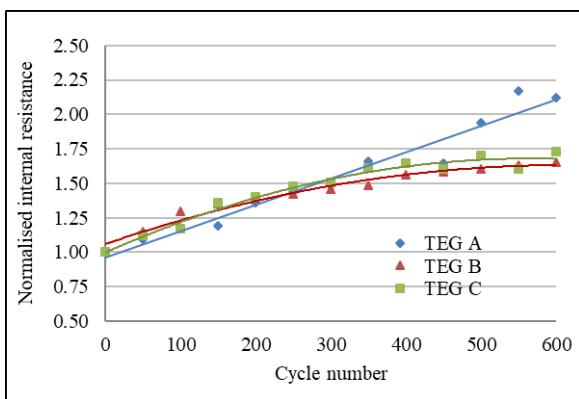

Figure 13: Evolution of the normalised internal resistance for each TEG over 600 thermal cycles

4.2.3 Effective Seebeck coefficient, α_{eff}

Figure 14 plots the calculated effective Seebeck coefficient obtained during each characterisation test. Each data point represents the average effective Seebeck coefficient obtained across all load currents/resistances during a characterisation test. The profiles shown match

those observed for the open circuit voltage, since α_{eff} is calculated using Equation 13 and the temperature difference was maintained relatively constant across all characterisation tests. Except for a slight increase of α_{eff} during the 50 first cycles and the outlier data point for cycle 600 for TEG A, α_{eff} may be considered constant throughout the testing. If the first and the last values may be ignored, the average value α_{eff} is approximately 0.0445 V/K for TEG A, 0.0444 V/K for TEG B and 0.0442 V/K for TEG C. These values represent roughly a 20% difference compared with the 0.056 V/K value provided by the manufacturer. This difference is similar to that presented by Hsu et al. [28] and it is due to the thermal contact resistances and the difference in the testing conditions.
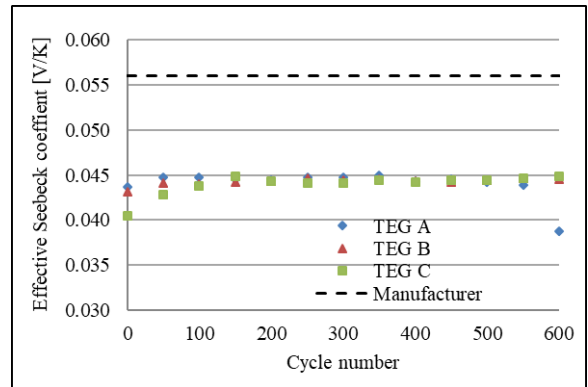

Figure 14: Evolution of the effective Seebeck cooefficient for each TEG over 600 cycles

4.3 Dimensionless Figure of Merit, ZT

The results of the Harman method testing performed on all TEGs with their 95% confidence bounds are listed in Table 6. The pre-cycling ZT values are in the expected range compared with the results of Barako et al. [14, 15]. The overall reduction in ZT drop is 81% for TEG A, 45% for TEG B and 39% for TEG C, again highlighting that TEG A suffers greater degradation due to higher frequency thermal cycling. It is noted that TEG C displayed larger variation in ZT value after 0 and 600 cycles, which may indicate some internal faults such as micro-cracks within the module.

An inspection of the Seebeck and Joule voltages between the pre-cycling and post-cycling tests finds that the decrease of ZT is predominantly due to the increase of the Joule voltage, while the Seebeck voltage remains constant in accordance with Figure 14. It can therefore be concluded that the decrease of the dimensionless figure of merit is mainly due to the increase of the internal resistance of the TEGs.

Table 6: Pre and post cycling dimensionless figure of merit values determined using the Harman method

	ZT before	ZT after	Change
A	0.616 ± 0.012	0.119 ± 0.007	↓81%
B	0.612 ± 0.023	0.336 ± 0.017	↓45%
C	0.609 ± 0.099	0.370 ± 0.152	↓39%

4.4 Cause of performance degradation

It is suggested that the increase in internal resistance of the TEGs and the corresponding decrease in ZT and power output is primarily a result of separation between material interfaces within the modules which is caused by thermal cycling. In particular, the semiconductor pellet/solder/copper junction is subjected to large stress imbalances owing to different physical properties. This leads to diffusion of the solder alloy and the formation of micro-cracks which have been observed in this region [13]. It is predicted that faster heating times result in greater thermal stresses and strain rates in the pellets and at the pellet/solder/copper junction, resulting in greater likelihood of crack formation and propagation and more rapid diffusion of the solder layer.

5. Future work

In this study, a constant current mode for the external load was employed during the thermal cycling tests. There are alternative approaches, such as maintaining the TEG in an open circuit condition. An electronic power converter controlled by a maximum power point tracking (MPPT) algorithm is another option as it would permit the observation of the degradation of the TEG and not also the increasing mismatch between the internal resistance of the TEG and external load resistances. However, this would make it more difficult to control the boundary temperatures so precisely. Regardless, a programmable external load controllable by PC would improve the rig capabilities and the time required to complete the necessary tests, and it may eliminate the recovery effect described previously. In this regard the recovery effect merits further study since there appears to be no references to this phenomenon in the literature. The inclusion of a pressure gauge/load cells in the experimental rig would be useful to observe with precision how the clamping pressure evolves over individual cycles and over the entire test campaign. The use of thermal interface materials such as pastes, or graphite foil could be employed to reduce thermal contact resistance and ensure greater temperature homogeneity on the faces of the TEG, though thermal pastes have been observed by some authors to pump out or dry out during repeated thermal cycling. SEM imaging of the TEG, as performed in some of the studies mentioned in the literature review would be useful to observe the effects of thermal cycling inside the TEG, but for sealed TEGs this is a destructive process which prevents the same TEG from being imaged both before and after testing. The results of the current study and future studies will form the basis of a degradation model that includes the various influencing parameters of material composition, pellet geometry, temperature limits, and cycling rates.

6. Conclusion

To investigate the effects of thermal cycling on thermoelectric generators, a bespoke experimental rig was developed. The power output and internal properties such as the Seebeck coefficient, the internal resistance and the dimensionless figure of merit were chosen to assess the evolution of generator performance. Three thermoelectric generators (TEGs) of the same make and model number were tested before, during and after 600 combined heating and cooling cycles. Each generator was subjected to a different thermal cycling regime. The only parameter varying between the regimes was the heating time, with average durations of 160 seconds for TEG A, 390 seconds for TEG B and 720 seconds for TEG C. It was observed that all samples demonstrated power generation performance reductions and the extent of the decrease was observed to correlate with faster heating times. It was observed that the decrease of the power output in the thermal cycling tests was not only due to the degradation of the generators but also to the mismatch of the resistances. The reduction of the maximum power output (at matched load) was determined to be 61% for TEG A, 34% for TEG B and 29% for TEG C.

It was observed that the heating times slightly decreased throughout the thermal cycling indicating a slight increase in the thermal resistance of the TEG modules. No significant change in the Seebeck coefficient value was observed, however a significant increase in the internal resistance of the generators was observed, respectively 2.15, 1.65 and 1.70 times their initial magnitude after 600 thermal cycling for TEGs A, B and C. The dimensionless figure of merit reduction after 600 thermal cycles was observed to be 81% for TEG A and 45 % for TEG B, and 39% for TEG C, and was attributed only to the increase of the internal resistance of the thermoelectric generators, which is predicted to arise from separation between material interfaces within the module and diffusion of the solder layer.

Nomenclature

Symbol	Description	Unit
A	Pellet cross-sectional area	m^2
C_p	Specific heat capacity	J/kg·K
I	Current	A
K	Thermal conductance	W/K
K_u	Controller gain	-
K_P	Proportional gain	-
L	Pellet length	m
Q_H	TEG hot side heat flow	W
Q_C	TEG cold side heat flow	W
R	Electrical resistance of TEG	Ω
R_L	Electrical resistance of load	Ω
T_C	TEG cold side temperature	K
T_H	TEG hot side temperature	K
t_D	Derivative time	s
t_I	Integral time	s
ΔT_{TEG}	TEG temperature difference	K
V	Voltage	V
V_{Joule}	Voltage due to Joule effect	V
V_{OC}	Open circuit voltage	V
$V_{Seebeck}$	Voltage due to Seebeck effect	V
W	Electrical power	W
W_{MAX}	Maximum electrical power	W
Z	Figure of merit	1/K
ZT	Dimensionless figure of merit	-
α	Seebeck co-efficient	V/K
α_{eff}	Effective Seebeck coefficient	V/K
λ	Thermal conductivity	W/m·K

| ρ | Density | kg/m^3 |
| σ | Electrical conductivity | S/m |

References
[1] Aranguren P, Astrain D, Pérez MG. Computational and experimental study of a complete heat dissipation system using water as heat carrier placed on a thermoelectric generator. Energy. 2014;74:346-58.

[2] Cataldo RL, Bennett GL. US Space Radioisotope Power Systems and Applications: Past, Present and Future. 2011.

[3] Jeng T-M, Tzeng S-C, Yang B-J, Li Y-C. Design, Manufacture and Performance Test of the Thermoelectric Generator System for Waste Heat Recovery of Engine Exhaust. Inventions. 2016;1:2.

[4] Champier D. Thermoelectric generators: A review of applications. Energy Conversion and Management. 2017;140:167-81.

[5] Nuwayhid RY, Shihadeh A, Ghaddar N. Development and testing of a domestic woodstove thermoelectric generator with natural convection cooling. Energy Conversion and Management. 2005;46:1631-43.

[6] Codecasa MP, Fanciulli C, Gaddi R, Gomez-Paz F, Passaretti F. Update on the Design and Development of a TEG Cogenerator Device Integrated into Self-Standing Gas Heaters. 2013:1-6.

[7] Børset MT, Wilhelmsen Ø, Kjelstrup S, Burheim OS. Exploring the potential for waste heat recovery during metal casting with thermoelectric generators: On-site experiments and mathematical modeling. Energy. 2017;118:865-75.

[8] Savani I, Waage MH, Børset M, Kjelstrup S, Wilhelmsen Ø. Harnessing thermoelectric power from transient heat sources: Waste heat recovery from silicon production. Energy Conversion and Management. 2017;138:171-82.

[9] Mirhosseini M, Rezania A, Rosendahl L, Iversen BB. Effect of Thermal Cycling on Zinc Antimonide Thin Film Thermoelectric Characteristics. Energy Procedia. 2017;142:519-24.

[10] Chen L, Lee J. Effect of pulsed heat power on the thermal and electrical performances of a thermoelectric generator. Applied Energy. 2015;150:138-49.

[11] Hori Y, Kusano D, Ito T, Izumi K. Analysis on thermo-mechanical stress of thermoelectric module. Thermoelectrics, 1999 Eighteenth International Conference on: IEEE; 1999. p. 328-31.

[12] Gao Y, Marconnet AM, Panzer MA, LeBlanc S, Dogbe S, Ezzahri Y, Shakouri, A, Goodson, KE. Nanostructured Interfaces for Thermoelectrics. Journal of Electronic Materials. 2010;39:1456-62.

[13] Hatzikraniotis E, Zorbas K, Samaras I, Kyratsi T, Paraskevopoulos K. Efficiency study of a commercial thermoelectric power generator (TEG) under thermal cycling. Journal of Electronic Materials. 2010;39:2112-6.

[14] Barako MT, Park W, Marconnet AM, Asheghi M, Goodson KE. A reliability study with infrared imaging of thermoelectric modules under thermal cycling. Thermal and Thermomechanical Phenomena in Electronic Systems (ITherm), 2012 13th IEEE Intersociety Conference on: IEEE; 2012. p. 86-92.

[15] Barako MT, Park W, Marconnet AM, Asheghi M, Goodson KE. Thermal Cycling, Mechanical Degradation, and the Effective Figure of Merit of a Thermoelectric Module. Journal of Electronic Materials. 2013;42:372-81.

[16] Park W, Barako MT, Marconnet AM, Asheghi M, Goodson KE. Effect of thermal cycling on commercial thermoelectric modules. Thermal and Thermomechanical Phenomena in Electronic Systems (ITherm), 2012 13th IEEE Intersociety Conference on: IEEE; 2012. p. 107-12.

[17] Tatarinov D, Wallig D, Bastian G. Optimized characterization of thermoelectric generators for automotive application. Journal of electronic materials. 2012;41:1706-12.

[18] de Cerqueira Veras JC, Vieira DA, Melo EC, de Souza CP. An automatic thermal cycling based test platform for thermoelectric generator testing. Instrumentation and Measurement Technology Conference (I2MTC), 2015 IEEE International: IEEE; 2015. p. 1949-53.

[19] Tenorio HCRL, Vieira DA, De Souza CP, De Macedo ECT, Freire RCS. A thermoelectric module thermal-cycling testing platform with automated measurement capabilities. 2016.

[20] Tenorio HCRL, Vieira DA, De Souza CP. Measurement of parameters and degradation of thermoelectric modules. IEEE Instrumentation & Measurement Magazine. 2017;20:13-9.

[21] Ding LC, Akbarzadeh A, Date A. Performance and reliability of commercially available thermoelectric cells for power generation. Applied Thermal Engineering. 2016;102:548-56.

[22] Patel VK, Wang H, Gluesenkamp KR, Gehl A, Ormston G, Kirkman E. Long-Term Effects of Power Quality and Power Cycling on Thermoelectric Module Performance. 2018:V001T04A8.

[23] Rowe DM. Thermoelectric power generation. Proceedings of the Institution of Electrical Engineers. 1978;125:1113-36.

[24] Bell LE. Cooling, heating, generating power, and recovering waste heat with thermoelectric systems. Science. 2008;321:1457-61.

[25] Hodes M. On one-dimensional analysis of thermoelectric modules (TEMs). IEEE Transactions on Components and Packaging Technologies. 2005;28:218-29.

[26] Tachibana M, Fang J. An Estimation of Thermal Stress of Thermoelectric Devices in the Temperature Cycling Test. Procedia Engineering. 2012;27:177-85.

[27] Zorbas K, Hatzikraniotis E, Paraskevopoulos KM. Power and Efficiency Calculation and Evaluation of Material Properties in Thermoelectric Power Generators. MRS Proceedings. 2011;1044:1044-U09-15.

[28] Hsu CT, Huang GY, Chu HS, Yu B, Yao DJ. An effective Seebeck coefficient obtained by experimental

results of a thermoelectric generator module. Applied Energy. 2011.

[29] Deasy MJ, Baudin N, O'Shaughnessy SM, Robinson AJ. Simulation-driven design of a passive liquid cooling system for a thermoelectric generator. Applied Energy. 2017;205:499-510.

[30] Thermalforce. TEG 127-200-24. Thermalforce.

[31] O'Shaughnessy SM, Deasy MJ, Doyle JV, Robinson AJ. Adaptive design of a prototype electricity-producing biomass cooking stove. Energy for Sustainable Development. 2015;28:41-51.

[32] Ming T, Wang Q, Peng K, Cai Z, Yang W, Wu Y, Gong T. The influence of non-uniform high heat flux on thermal stress of thermoelectric power generator. Energies. 2015;8:12584-602.

[33] O'Shaughnessy SM, Deasy MJ, Doyle JV, Robinson AJ. Field trial testing of an electricity-producing portable biomass cooking stove in rural Malawi. Energy for Sustainable Development. 2014;20:1-10.

[34] Ziegler-Nichols Autotuning Method. National Instruments.http://zone.ni.com/reference/en-XX/help/370401J-01/lvpidmain/ziegnichforms/. Accessed on 18th November 2018.

[35] Deasy MJ, O'Shaughnessy SM, Archer L, Robinson AJ. Electricity generation from a biomass cookstove with MPPT power management and passive liquid cooling. Energy for Sustainable Development. 2018;43:162-72.

[36] Jacquot A, Jägle M, König J, Ebling D, Böttner H. Theoretical study of the Harman method for evaluating the thermoelectric performance of materials and components at high temperature. Proceedings of the 5th European Conference on Thermoelectrics2007.